


## Phase diagram of the $(\text{Pr}_{1-y}\text{Sm}_y)_{0.7}\text{Ca}_{0.3}\text{CoO}_3$ system: Valence and spin state transition versus ferromagnetism

Y. Bréard, F. Veillon, L. Hervé, and V. Hardy <sup>\*</sup>

Normandie Université, École nationale supérieure d'ingénieurs de Caen (ENSICAEN), Université de Caen Normandie (UNICAEN),  
Centre national de la recherche scientifique (CNRS), CRISMAT, 14000 Caen, France

F. Guillou 

Inner Mongolia Key Laboratory for Physics and Chemistry of Functional Materials, Inner Mongolia Normal University,  
81 Zhaowuda Road, Hohhot 010022, Inner Mongolia, People's Republic of China

K. Kummer , F. Wilhelm , and A. Rogalev

European Synchrotron Radiation Facility (ESRF), 71 Avenue des Martyrs, F-38000 Grenoble, France

R. I. Smith 

Rutherford Appleton Lab, ISIS Pulsed Neutron & Muon Source, Harwell Campus, Didcot OX11 0QX, Oxon, United Kingdom



(Received 21 October 2021; accepted 16 December 2021; published 5 January 2022)

The valence and spin-state transition is a very specific transition found in some cobalt oxides which involves a coupled modification in the Co valence and the  $\text{Co}^{3+}$  spin state. In the phase diagram of these compounds, one can thus expect a competition of this transition with the ferromagnetism associated with  $\text{Co}^{4+}$  low spin/ $\text{Co}^{3+}$  high spin double exchange. Here, we study the phase diagram of  $(\text{Pr}_{1-y}\text{Sm}_y)_{0.7}\text{Ca}_x\text{CoO}_3$  and  $\text{Pr}_{1-x}\text{Ca}_x\text{CoO}_3$  to shed some light on the competition between these two phenomena. To this end, we combine results obtained with a wide variety of techniques: magnetization, heat capacity, resistivity, neutron diffraction, x-ray absorption spectroscopy, and x-ray magnetic circular dichroism. The origin of the various transition lines in the phase diagram of  $(\text{Pr}_{1-y}\text{Sm}_y)_{0.7}\text{Ca}_3\text{CoO}_3$  as well as that of the critical value  $y_{\text{crit}} \sim 0.18$  are discussed. Particular attention is paid to the nature of the ground state magnetism which is an issue strongly debated so far in this type of cobaltate.

DOI: [10.1103/PhysRevMaterials.6.014401](https://doi.org/10.1103/PhysRevMaterials.6.014401)

### I. INTRODUCTION

A very peculiar type of transition is observed in some cobalt oxides, showing a concomitant change in the valence ( $\text{Co}^{3+}/\text{Co}^{4+}$ ) and in the spin state [ $\text{Co}^{3+}$  low spin (LS)/ $\text{Co}^{3+}$  high spin (HS)] degrees of freedom. Since being discovered in well-oxygenated  $\text{Pr}_{0.5}\text{Ca}_{0.5}\text{CoO}_3$  [1–5] (for an overview, see for instance Ref. [6] and references therein), the field of such a valence and spin-state transition (VSST) was progressively extended to a broader range of compositions, namely,  $(\text{Pr}_{1-y}\text{RE}_y)_{1-x}\text{Ca}_x\text{CoO}_3$  with  $\text{RE} = \text{Sm}, \text{Eu}, \text{Gd}, \text{Tb}, \text{or Y}$  and  $0.2 \leq x \leq 0.5$  as well as  $0.0 \leq y \leq 0.3$  [7–12].

In a study on  $\text{Pr}_{0.5}\text{Ca}_{0.5}\text{CoO}_3$ , Tsubouchi *et al.* [1] reported a metal-insulator transition accompanied by an abrupt drop in magnetization, a sharp peak in specific heat, and a decrease in the unit cell volume, when cooling below the transition at  $T^* \sim 90$  K. Originally, this transition was regarded as a peculiar instance of a first-order spin-state transition (SST) among the  $\text{Co}^{3+}$  (from intermediate-spin to LS state), an interpretation that remained commonly accepted for several years. However, an accumulation of data pointed to a more

complex scenario. First, in a neutron powder diffraction study of  $\text{Pr}_{0.5}\text{Ca}_{0.5}\text{CoO}_3$ , Barón-González *et al.* [2] observed that the Co-O bonds were almost unaltered at  $T^*$ , whereas the Pr-O ones changed a lot, a result leading them to suggest the possibility of a charge transfer between Co and Pr. Soon after, in their study of the heat capacity in  $(\text{Pr}_{1-y}\text{Y}_y)_{0.7}\text{Ca}_{0.3}\text{CoO}_3$  compounds, Hejtmánek *et al.* [10] found a Schottky-like anomaly at  $T < T^*$ , a feature suggesting the presence of the Kramers ion  $\text{Pr}^{4+}$ . Then several experiments of x-ray absorption spectroscopy (XAS) provided direct evidence of the presence of  $\text{Pr}^{4+}$  below  $T^*$  in different compounds. In  $\text{Pr}_{0.5}\text{Ca}_{0.5}\text{CoO}_3$ , for instance, García-Muñoz *et al.* [3] and Herrero-Martín *et al.* [4] both demonstrated a partial oxidation of  $\text{Pr}^{3+}$  into  $\text{Pr}^{4+}$  when crossing  $T^*$  upon cooling.

The fact that the VSST requires the stabilization of a certain amount of  $\text{Pr}^{4+}$  at low temperatures is now widely accepted [2,3,10,13]. However, the very origin of such a mixed valence  $\text{Pr}^{3+}/\text{Pr}^{4+}$  is still a matter of debate. On the experimental side, the data on the value of this ratio are scarce and rather scattered. The only point that emerges clearly is that, for a given (RE,  $x$ ) couple, the ratio  $\text{Pr}^{4+}/\text{Pr}$  increases with  $y$  [10,12,14]. Experimentally, another basic issue is the competition between the VSST and the ferromagnetic (FM) ordering. In  $(\text{Pr}_{1-y}\text{RE}_y)_{1-x}\text{Ca}_x\text{CoO}_3$ , one expects

<sup>\*</sup>vincent.hardy@ensicaen.fr

a critical  $y$  value ( $y_{\text{crit}}$ ) below which FM (related to that of  $\text{Pr}_{1-x}\text{Ca}_x\text{CoO}_3$ ) dominates and above which the VSST takes place. Even though one can expect a link between  $y_{\text{crit}}$  and the  $\text{Pr}^{4+}$  content in the ground state, a precise description of the crossover FM/V SST is still missing.

These various issues are addressed in this paper. Our study was carried out in the  $(\text{Pr}_{1-y}\text{Sm}_y)_{0.7}\text{Ca}_{0.3}\text{CoO}_3$  system, which is well suited for an experimental investigation of the VSST. Indeed, owing to its size—slightly smaller than that of  $\text{Pr}^{3+}\text{—Sm}^{3+}$  offers the best fine control of the VSST, even though its magnetic response must be considered in the analysis. A series of measurements have been conducted as a function of  $y$ : magnetic susceptibility, heat capacity, and resistivity as well as isothermal magnetoresistance (MR) and magnetization curves. From these data, the  $y$  dependencies of several characteristic temperatures have been derived: Curie temperature ( $T_C$ ), temperature of VSST ( $T^*$ ), and temperature of short-range ordering (SRO) of FM clusters ( $T_{\text{SRO}}$ ). The exploration of physical properties was complemented by experiments of XAS to characterize the  $\text{Pr}^{4+}/\text{Pr}$  ratio (at 5 K) and magnetic circular dichroism (XMCD) to address the spin state of  $\text{Co}^{3+}$ . On this basis, we discuss an overall description of the phase diagram, with special attention paid to the boundary between the FM and VSST regimes.

## II. EXPERIMENTAL DETAILS

Polycrystalline samples of  $(\text{Pr}_{1-y}\text{Sm}_y)_{0.7}\text{Ca}_{0.3}\text{CoO}_3$ , with 12 compositions in the range  $0 \leq y \leq 0.5$  were prepared by solid-state reaction, in a way like that previously used for  $y = 0.3$  [15–18]. Starting from stoichiometric proportions of  $\text{Pr}_6\text{O}_{11}$ ,  $\text{Sm}_2\text{O}_3$ ,  $\text{CaO}$ , and  $\text{Co}_3\text{O}_4$  precursors, the powders were intimately ground, and the mixture was pelletized in the form of  $2 \times 2 \times 10$  mm bars. These bars were first sintered at 1200 °C in flowing oxygen for 30 h and then annealed in high-pressure (130 bar)  $\text{O}_2$  atmosphere for 80 h at 650 °C with the aim of ensuring good oxygenation of the samples.

By nature, the VSST samples entangle steric and doping effects: the former originates from the size difference between  $\text{Pr}^{3+}$  and  $\text{Sm}^{3+}$ , while the latter results from the impact of a  $\text{Pr}^{4+}/\text{Pr}^{3+}$  fraction on the  $\text{Co}^{4+}/\text{Co}^{3+}$  ratio (via charge balance). Accordingly, a second series  $\text{Pr}_{1-x}\text{Ca}_x\text{CoO}_3$  ( $x < 0.4$ ) was investigated to isolate the role of the doping per se (there is no VSST for this  $x$  range). Using stoichiometric mixtures of the same precursors, the bars were first sintered at 1000 °C in air for 24 h and then annealed in flowing oxygen for 24 h at 1200 °C before being cooled down to room temperature in 40 h. The procedure was repeated twice after grinding and repelletization of the samples. Lastly, we prepared the compound  $\text{Pr}_{0.7}\text{Ca}_{0.3}\text{Ga}_{0.7}\text{Ti}_{0.3}\text{O}_3$  to get a direct estimate of the  $\text{Pr}^{3+}$  magnetism in the  $(\text{Pr}_{1-y}\text{Sm}_y)_{0.7}\text{Ca}_{0.3}\text{CoO}_3$  series. With  $\text{Ga}^{3+}$  and  $\text{Ti}^{4+}$  at the B sites, the only magnetic cation is  $\text{Pr}^{3+}$  at the A sites, and by keeping the same  $x = 0.3$   $\text{Ca}^{2+}$  content on the A site, the  $\text{Pr}^{3+}$  environment will be like that in our Co-containing compounds. The synthesis procedure was previously described in Ref. [18].

To check the purity of the samples, x-ray diffraction was performed on a X'pert Pro PANalytical diffractometer ( $K_\alpha$  Cu = 1.549 Å), equipped with an X'Celerator detector. For a more detailed structure investigation, time-of-flight

powder neutron diffraction (tofPND) data were collected at room temperature on the medium-resolution, high-count rate Polaris diffractometer [19] at the ISIS facility, Rutherford Appleton Laboratory, UK.

Here, 6 g of each sample were loaded into an 8-mm-diameter thin-walled cylindrical vanadium sample can and mounted on the beamline's automated sample changer. Neutron diffraction data were collected simultaneously in all five Polaris detector banks for a total proton beam charge to the ISIS target of 150  $\mu\text{Ah}$  ( $y = 0$ ) or 400  $\mu\text{Ah}$  ( $y \neq 0$ )—where 180  $\mu\text{Ah}$  is equivalent to  $\sim 1$  h exposure in the neutron beam. For data reduction, we used MANTID software [20], with normalized diffraction patterns from banks 1, 2, and 3 used in structure refinement (average  $2\theta$  scattering angles  $\sim 10^\circ$ ,  $26^\circ$ , and  $52^\circ$ , respectively).

For crystal structure refinement by Rietveld profile analysis, we used the FULLPROF suite of programs [21]. The neutron scattering lengths used were those included in the software, and a cylindrical sample absorption correction was applied during the refinements to account for the large wavelength-dependent neutron absorption cross-section of Sm in samples with  $y \neq 0$  ( $\sigma_a \sim 5900$  barns at  $\lambda = 1.8$  Å).

The magnetic data were collected using a superconducting quantum interference device magnetometer (MPMS, Quantum Design), while the heat capacity and resistivity measurements were carried out by means of a multipurpose instrument (PPMS, Quantum Design). In addition to the temperature dependencies (2–400 K) of all these quantities, the field dependence of magnetization and resistivity was investigated in the ground state ( $T = 5$  K).

X-ray absorption experiments at the Pr  $L_3$  and Co  $K$  edges were carried out at the ID12 beamline of the European Synchrotron (ESRF) in a multipurpose end station [22]. The sample was mounted on a cold finger cryostat, allowing the temperature of the sample to vary in the range 2.1–320 K. Partial fluorescence yield was collected in backscattering geometry using a Silicon Drift Detector mounted at  $20^\circ$  with respect to the incident beam.

XAS and XMCD experiments at the Co  $L_{2,3}$  edges presented in the Supplemental Material [23] were carried out at the ID32 beamline of the ESRF. The experimental end station allowed us to reach magnetic fields up to 9 T and temperature on the sample down to 5 K [24]. Bulk polycrystalline samples ( $\sim 2 \times 2 \times 5$  mm<sup>3</sup>) were cleaved in an ultrahigh vacuum chamber before being transferred to the superconducting magnet. XMCD spectra were recorded by flipping both the helicity of the incoming beam and the magnetic field direction.

## III. RESULTS

### A. Structural features

TofPND experiments in  $(\text{Pr}_{1-y}\text{Sm}_y)_{0.7}\text{Ca}_{0.3}\text{CoO}_3$  have been carried out at room temperature for  $y = 0, 0.075, 0.15, 0.25,$  and  $0.4$ . All the Rietveld refinements were successfully conducted with the  $Pnma$  space group that is expected for distorted perovskites. The Pr, Sm, and Ca atoms were found to be statistically distributed over the same crystallographic site, without any indication of ordering phenomena. In agreement with previous studies, Fig. 1(a) shows that the unit

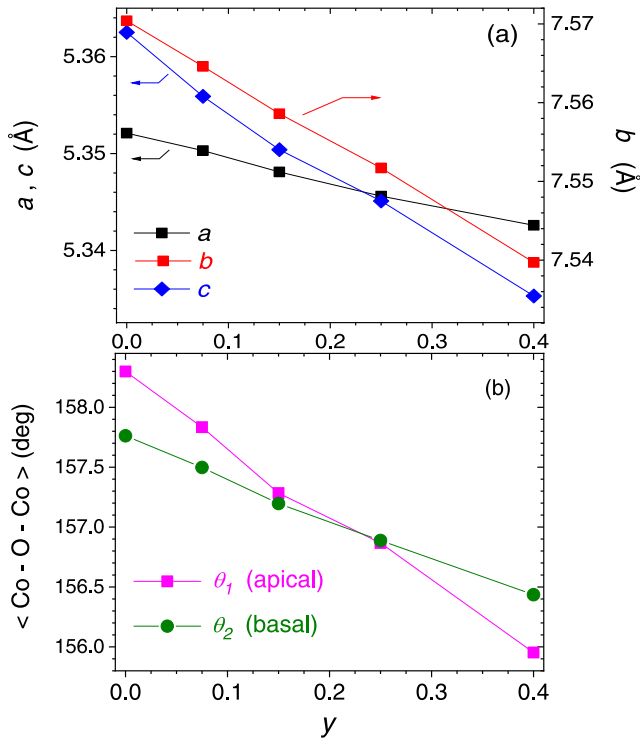


FIG. 1. Results of time-of-flight powder neutron diffraction (tofPND) investigations of  $(\text{Pr}_{1-y}\text{Sm}_y)_{0.7}\text{Ca}_{0.3}\text{CoO}_3$  at room temperature. (a) Unit cell parameters as a function of  $y$  ( $Pnma$  space group). (b) Apical and basal Co-O-Co angles as a function of  $y$ .

cell parameters decrease continuously when  $y$  increases, as expected from the smaller size of  $\text{Sm}^{3+}$  (1.132 Å) than that of  $\text{Pr}^{3+}$  (1.179 Å) [8,25]. Due to the differences in relative atomic scattering powers between neutrons and x rays, neutron diffraction allows us to determine much more precisely the oxygen atoms positions and therefore the Co-O-Co angles, which directly reflect the degree of distortion of the perovskite (see details in the Supplemental Material [23]). The angle  $\theta_1$  refers to the Co-O1-Co angle involving the apical oxygen atoms, while  $\theta_2$  refers to the Co-O2-Co angle involving the basal oxygen atoms. Figure 1(b) shows that both angles decrease linearly with the increase of Sm content.

### B. Physical properties

Figure 2 shows magnetization curves divided by the applied field (5 T) for all values of  $y$  [26]. A crossover from the FM to the VSST regime for  $0.175 < y < 0.19$  is evident. In such a high field, the signature of  $T^*$  remains well defined, whereas the FM transition is broadened (a much smaller field will be used to define the  $T_C$ , as detailed hereafter). The inset of Fig. 2 displays an enlargement of the reciprocal susceptibility around room temperature, which shows a Curie-Weiss (CW)-like form. One also notes a substantial decrease of susceptibility as  $y$  is increased.

Figure 3 shows the heat capacity curves for selected values of  $y$ . A clear peak attributed to the VSST is visible for the largest  $y$  values ( $>0.15$ ). In contrast, no clear feature emerges on the  $C(T)$  of the compositions ( $\leq 0.15$ ) situated in the FM regime (see enlargements in the Supplemental Material [23]).

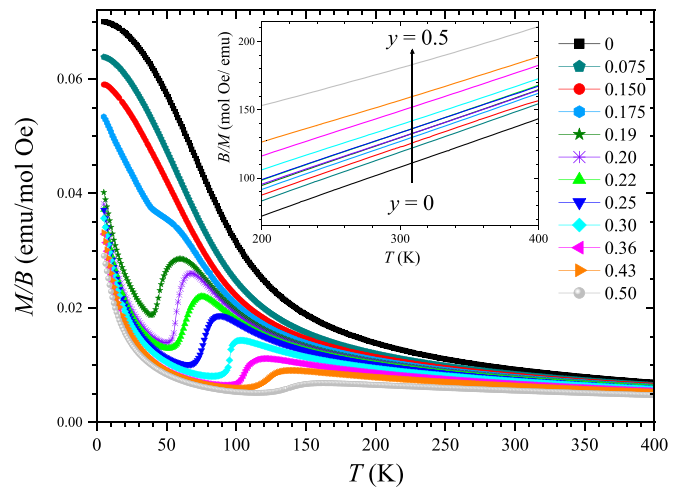


FIG. 2. Ratio of the magnetization to the applied field (5 T) as a function of the temperature, for all the investigated  $y$  values. The inset shows the reciprocal within the high- $T$  range.

It can be noted that the peak at  $T^*$  exhibits a maximum of sharpness at  $y \sim 0.3$ , a feature previously observed by Fujita *et al.* [8] in this  $(\text{Pr}_{1-y}\text{Sm}_y)_{0.7}\text{Ca}_{0.3}\text{CoO}_3$  system. It also deserves to be noted that, for small  $y$  values, the low- $T$  part of the curves appears as a smooth extrapolation of the high- $T$  regime (following a Debye-like shape), whereas the high- $y$  curves exhibit a downward shift below  $T^*$ . This can be ascribed to the fact that the VSST is accompanied by a decrease in the unit cell volume upon cooling [1,2,7,27]. This induces an increase in Debye temperature when cooling below  $T^*$  and thus a negative step in the lattice contribution (which is the greatest part of the baseline onto which the VSST peak is superimposed). The inset of Fig. 3 displays a  $C/T$  vs  $T^2$  plot of the data within the low- $T$  range. For  $y = 0$ , one observes a straight line which indicates a response essentially made of a lattice term and an electronic one. A strong change takes place when increasing  $y$ , especially at the crossover FM/VSST: in

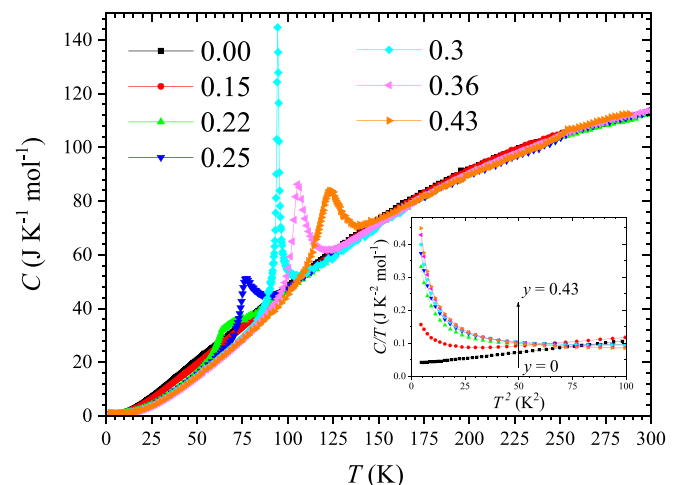


FIG. 3. Heat capacity as a function of temperature, for selected  $y$  values. The inset shows the ratio  $C/T$  vs  $T^2$  at  $T \leq 10$  K. See the Supplemental Material [23] for details in the  $C(T)$  curves for  $y \leq 0.15$  and  $T \leq 120$  K.

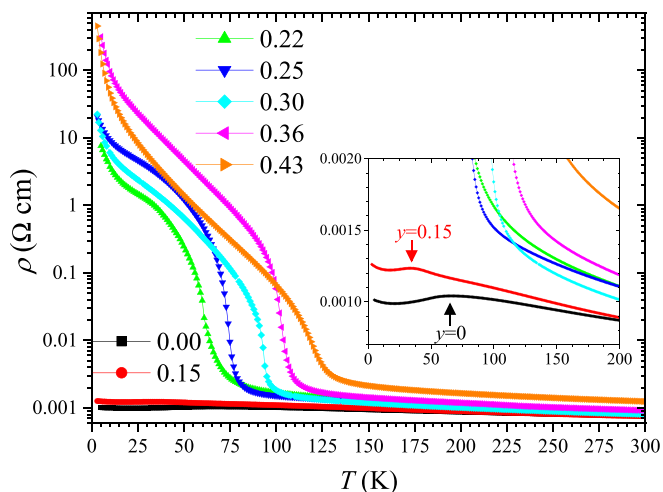


FIG. 4. Resistivity (log scale) as a function of temperature, for selected values of  $y$ . The inset is an enlargement (linear scale) for the two lowest  $y$  values, whose curves exhibit a broad hump (marked by arrows).

addition to a decrease in the lattice term, the most prominent effect is the emergence of a Schottky peak (actually only its high- $T$  wing is visible in our  $T$  range) that is ascribable to  $\text{Sm}^{3+}$  ( $y = 0.15$ ) as well as to the VSST-induced  $\text{Pr}^{4+}$  (for  $y > 0.15$ ), which are both Kramers ions.

Figure 4 shows the resistivity of selected  $y$  values in a semilogarithmic plot. The most salient feature is a sudden increase in resistivity upon cooling for the highest  $y$  values (those in the VSST regime). This transition corresponds to  $T^*$ , and these compounds reach at low- $T$  a resistivity at least four orders of magnitude higher than in low- $y$  compounds. The latter exhibit a weak resistivity over the whole temperature range, which can even be regarded as a metallic one [28]. One can also note that these curves exhibit a flat maximum within the low- $T$  range, i.e., there is a regime of decreasing resistivity upon cooling (see inset). Such a feature can be related to a FM transition based on a double-exchange (DE) mechanism [29].

In Fig. 5, we gather data about the field dependence of the ground state. Figure 5(a) shows the central part of  $M$  ( $B$ : 5 T  $\rightarrow$  -5 T  $\rightarrow$  5 T) recorded at 5 K for the whole  $y$  series. In the FM regime, one observes hysteresis loops with sizeable values of remanence and coercive field. The high- $B$  part keeps a positive slope until 5 T, while its height is slightly shifted downward as  $y$  is increased. For  $y > 0.175$ , the crossover to VSST regime is quite clear, leading to  $M(B)$  curves virtually reversible (e.g., for  $y = 0.3$ , a remanent magnetization of  $0.003 \mu_B/\text{f.u.}$  and a coercive field of 80 Oe). In other respects, these curves still exhibit a marked, monotonous increase with the field. In Fig. 5(a), one of the most striking features is the absence of saturation in the FM regime, which persists up to at least 14 T (see the Supplemental Material [23]). This behavior is in line with previous studies, and it can be at least partly ascribed to the rare-earth (RE) magnetism.

Figure 5(b) shows the field dependence of the MR  $\{\text{MR} = [\rho(B) - \rho(0)]/\rho(0)\}$  recorded at 5 K within the  $y$  series (measuring path  $+9 \text{ T} \rightarrow -9 \text{ T}$ ). The crossover FM/VSSST has a very visible impact, inducing changes in both the shape and

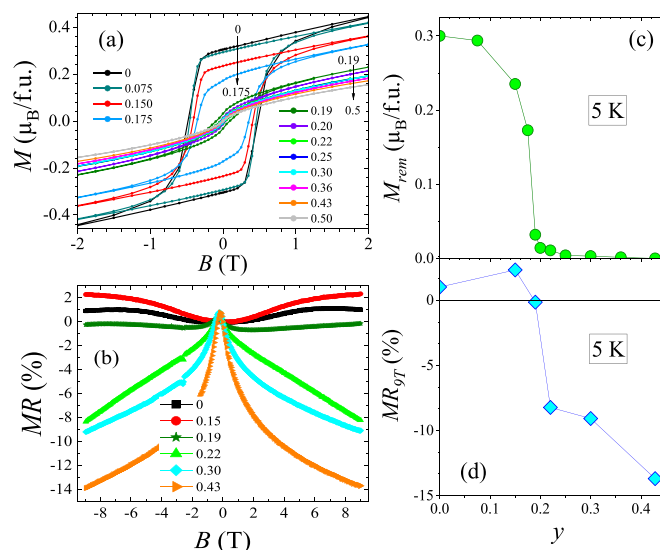


FIG. 5. (a) Magnetic hysteresis loops at 5 K for all the  $y$  values. (b) Magnetoresistance  $\{\text{MR} = 100[\rho(B) - \rho(0)]/\rho(0)\}$  at 5 K for selected values of  $y$ . (c) Remanent magnetization derived from (a) as a function of  $y$ . (d) MR at 9 T derived from (b) and plotted as a function of  $y$ .

sign of the  $\text{MR}(B)$  curves. The negative MR of the samples in the VSST regime is consistent with previous reports in related systems [30]; in contrast, the positive MR found at the FM side is much more unusual. Curiously, we were unable to find in the literature previous results on the MR at low- $T$  for  $y = 0$  ( $\text{Pr}_{0.7}\text{Ca}_{0.3}\text{CoO}_3$ ), despite the many studies carried out on this compound. For the  $y$  values of Fig. 5(b),  $\rho(B)$  curves were recorded at regularly spaced temperature up to 140 K. The curves  $\text{MR}(T)$  extracted from these data exhibit peaks located either at  $T_C$  or at  $T^*$ , depending on the  $y$  value (see the Supplemental Material [23]).

From Figs. 5(a) and 5(b), we derived the  $y$  dependencies of the remanent magnetization [Fig. 5(c)] and MR [Fig. 5(d)] at 5 K. In both cases, a sharp crossover takes place at a critical value  $y_{\text{crit}} \sim 0.18$ , separating the FM and VSST regimes.

### C. Phase diagram

The characteristic temperatures of the  $(\text{Pr}_{1-y}\text{Sm}_y)_{0.7}\text{Ca}_3\text{CoO}_3$  system were primarily derived from magnetic measurements, which led us to address the impact of the following three issues: value of the measuring field, hysteresis, and training effect (see the Supplemental Material [23]). The latter stems from the first-order nature of the VSST, which requires the sample to accommodate the structural distortion at the transition. In such a case, several crossings of the transition can be necessary before finding a reproducible transition path. In our compounds, this effect was found to be limited to the first cooling, which was thus systematically discarded from our analysis. The hysteresis across the VSST is still an active subject of debate. It is now admitted that it is not as high as initially reported, and it is very dependent on the sweep rate [31]. It remains that a small hysteresis seems to persist even for quasistatic measurements, especially in the case of the lowest  $T^*$ , i.e., for the lowest  $y$

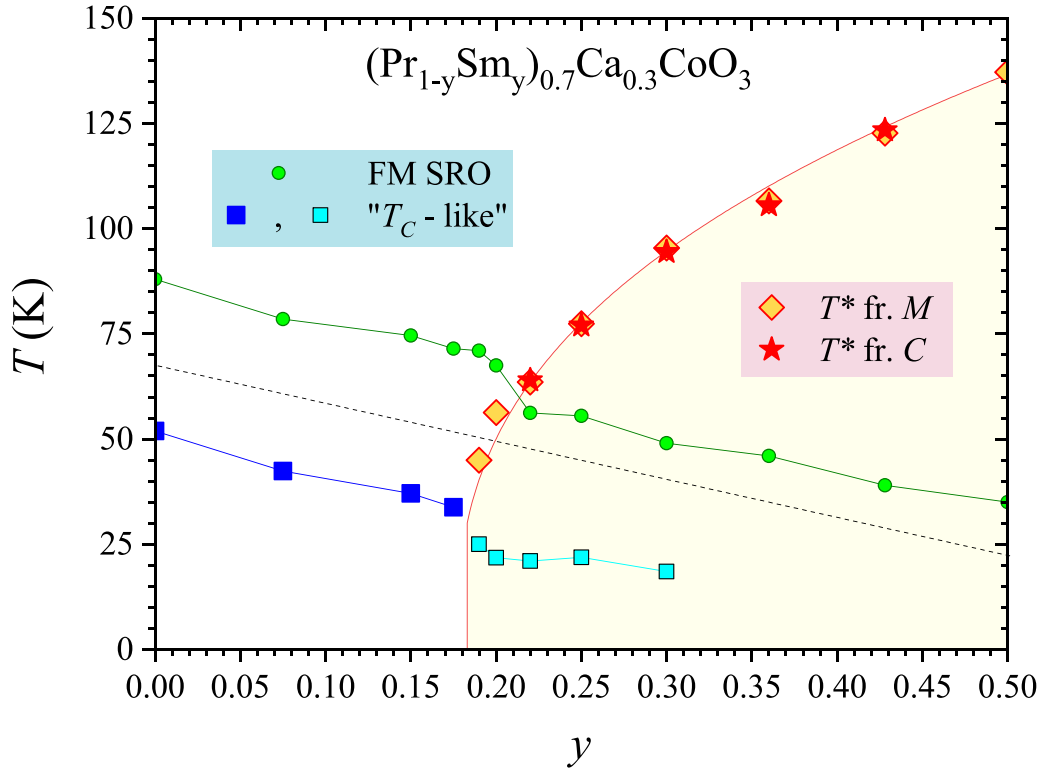


FIG. 6. Phase diagram of the system  $(\text{Pr}_{1-y}\text{Sm}_y)_{0.7}\text{Ca}_{0.3}\text{CoO}_3$ . See the Supplemental Material [23] for illustrations of the criteria used to determine the characteristic temperatures. The  $T^*$  line is derived both from the position of the inflection point on the  $M(T)$  curves and that of the peak on the  $C(T)$  ones. The thin red line is a fitting function of the form  $(y - y_{\text{crit}})^n$  (see text). The ferromagnetic (FM) short-range ordering (SRO) line is derived from the kink on  $dM_{\text{spont}}/dT$  (where  $M_{\text{spont}}$  is the spontaneous magnetization measured upon cooling in a field of  $\sim 1.5$  Oe). The squares are ascribed to the predominant Curie temperature of the distribution of FM clusters. These characteristic temperatures are derived from the presence of a minimum in  $[dM_{\text{spont}}/dT](T)$ . On the low- $y$  side, it simply reflects the midpoint of the FM ordering (absolute minimum in  $dM_{\text{spont}}/dT$ ), whereas it rather corresponds to a local minimum for larger  $y$  values. The dashed line shows the expected  $dT_C/dy$  calculated from data of the literature on cobaltates (see Sec. IV A 2).

values [31,32]. To avoid related scattering, we considered the field-cooled warming (FCW) mode at a rate of 0.5 K/min. The value of the measuring field only weakly impacts the  $T^*$ , whereas it is mandatory to use a low field to get a reliable value of  $T_C$ . For this purpose, we used either 10 Oe in FCW mode or, preferably, the inspection of the spontaneous magnetization ( $M_{\text{spont}}$ ), i.e., when cooling in the residual field of the superconducting coil after demagnetization ( $\sim 1.5$  Oe).

In our phase diagram, the characteristic temperatures are based on the derivative of  $M_{\text{spont}}$  (see the Supplemental Material [23]). A negative maximum of  $dM_{\text{spont}}/dT$  was ascribed to  $T_C$ ; this definition is akin to the usual midpoint criterion applied to the rise of magnetization upon cooling. Since this feature is considerably weaker above  $y_{\text{crit}}$  than below it, the  $T_C(y)$  line will be divided into two parts. A positive maximum of  $dM_{\text{spont}}/dT$  is ascribed to  $T^*$ ; this reflects the positive step in (paramagnetic) magnetism that is associated with a change from  $(\text{Pr}^{4+}, \text{Co}^{3+} \text{ LS})$  to  $(\text{Pr}^{3+}, \text{Co}^{4+} \text{ LS}, \text{Co}^{3+} \text{ HS})$  when crossing  $T^*$  upon warming [16]. Finally, the  $T_{\text{SRO}}$  is connected to the takeoff of  $dM_{\text{spont}}/dT$  upon cooling; we found it also corresponds to the start of a nonlinear magnetic response.

The phase diagram resulting from these  $T_C(y)$ ,  $T^*(y)$ , and  $T_{\text{SRO}}(y)$  lines is shown on Fig. 6. We added to this plot the position of the maxima in  $C(T)$ , which can be regarded as another signature of  $T^*$ . The inflection points on the resistivity

curves are also found to be well consistent with these lines (see the Supplemental Material [23]).

#### D. Boundary FM/VSSST

The  $T^*(y)$  data are fitted to a function of the form  $(y - y_{\text{crit}})^n$ , leading to  $y_{\text{crit}} = 0.177$  and  $n = 0.38$ . Hereafter, we will keep the rounded value  $y_{\text{crit}} \sim 0.18$ . Let us emphasize that this  $y_{\text{crit}}$  marks a change in the hierarchy between the FM and VSST regimes, but the two transitions can coexist. This is evident on Fig. 7(a) in the case of  $y = 0.19$  ( $> y_{\text{crit}}$ ), where one can observe below  $T^*$  the signature of  $T_C$ , that is here clearly highlighted by the bifurcation between the ZFC and FCC branches. Very similar features were observed for  $y = 0.0625$  in the  $(\text{Pr}_{1-y}\text{Y}_y)_{0.7}\text{Ca}_3\text{CoO}_3$  system [32]. On the other side, Fig. 7(b) shows that a signature of  $T^*$  can be observed for  $y = 0.175$  ( $< y_{\text{crit}}$ ) when applying a magnetic field large enough to spread out the FM transition.

In mixed valent cobaltates, the FM response is intimately related to the  $\text{Co}^{3+}/\text{Co}^{4+}$  ratio. Since the  $y_{\text{crit}}$  value involves the strength of the FM response, it must be indirectly connected to the  $\text{Pr}^{4+}/\text{Pr}^{3+}$  ratio. A basic question is thus to tackle the intrinsic  $y$  dependence of this  $\text{Pr}^{4+}$  content at low- $T$ . To do so, XAS experiments is undoubtedly the most suited tool.

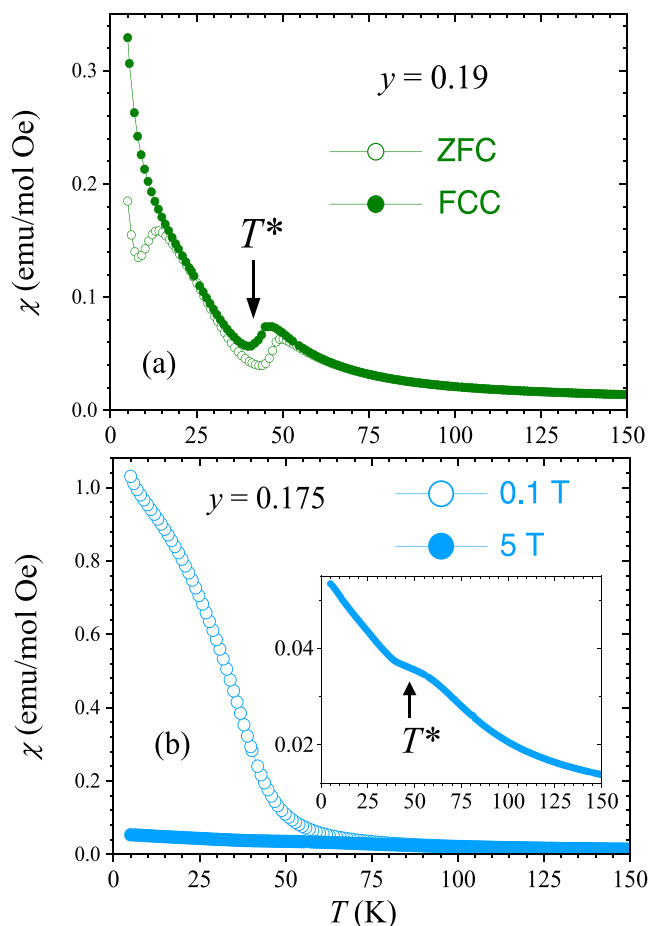


FIG. 7. Curves of dc susceptibility ( $M/B$ ) vs temperature: (a) zero-field-cooled and field-cooled cooling curves recorded in 0.1 T for  $y = 0.19$ . (b) Field-cooled cooling curves recorded in 0.1 and 5 T for  $y = 0.175$ . The inset is an enlargement of the high- $T$  curve revealing a signature of  $T^*$ .

### E. Pr valence at low $T$

Let us first summarize the literature on this issue. In the archetypical VSST compound  $\text{Pr}_{0.5}\text{Ca}_{0.5}\text{CoO}_3$ , a large range of values are reported ( $\text{Pr}^{4+}/\text{Pr}$  values at low  $T$  are between 0.15 [4] and 0.26 [3]). In  $(\text{Pr}_{1-y}\text{RE}_y)_{1-x}\text{Ca}_x\text{CoO}_3$  systems, the  $\text{Pr}^{4+}/\text{Pr}$  ratio was shown to increase with  $y$ ; this was studied in detail in the case  $x = 0.3$  for both Y and Tb: for  $\text{RE} = \text{Y}$ , when  $y$  is doubled from 0.075 to 0.15,  $\text{Pr}^{4+}/\text{Pr}$  goes from 0.15 to 0.27 [14]; for  $\text{RE} = \text{Tb}$ , when  $y$  is doubled from 0.1 to 0.2,  $\text{Pr}^{4+}/\text{Pr}$  goes from 0.19 to 0.25 [12].

In this paper, we address the case  $\text{RE} = \text{Sm}$ , with nine  $y$  values between 0 and 0.43. The Pr valence was determined from  $\text{Pr } L_3$  spectra using a method like that previously employed for VSST materials [3,4,6,14,18]. The  $\text{Pr } L_3$  edge was fitted by a combination of one arctangent (accounting for the edge jump), one Lorentzian forming the main white line representative of  $\text{Pr}^{3+}$ , and two Lorentzian functions representative of  $\text{Pr}^{4+}$  ( $\sim 5$  and 12 eV above the main white line), see spectral decomposition in Ref. [18]. The  $\text{Pr}^{4+}$  fraction was then calculated from the ratio of the integrated intensity of the Lorentzian functions. The results of  $\text{Pr}^{4+}/\text{Pr}$  vs  $y$  at  $T = 5$  K are shown in Fig. 8. As  $y$  is increased, the increase

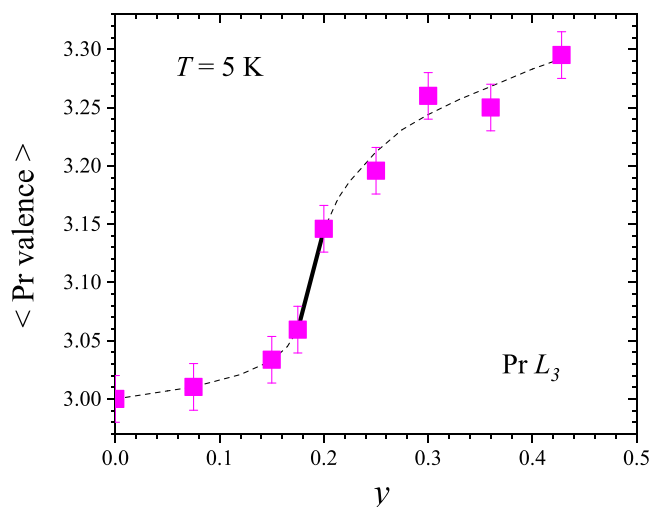


FIG. 8. Average Pr valence at 5 K, derived from the analysis of x-ray absorption spectroscopy (XAS) measurements at the  $\text{Pr } L_3$  edge. The dashed line is a guide to the eye. Note the presence of a weak but undeniable jump between  $y \sim 0.175$  and 0.20 (thick solid line).

in  $\text{Pr}^{4+}/\text{Pr}$  exhibits an S-like shape with an inflection point around  $y = 0.18$ , i.e., a value close to  $y_{\text{crit}}$ .

### F. Doping effect

The interest in the series  $\text{Pr}_{1-x}\text{Ca}_x\text{CoO}_3$  is to deconvolute the doping effect from the others in the analysis of the VSST transition. In this series, the doping corresponds to the ratio  $\text{Co}^{4+}/\text{Co}$  that is directly given by  $x$ . For sufficient level of doping, FM related to a DE mechanism between  $\text{Co}^{4+}$  and  $\text{Co}^{3+}$  takes place. In other respects, the  $\text{Co}^{3+}$  can undergo a SST from LS to HS as the temperature is increased.

Susceptibility curves were recorded for eight values of  $x$  in the range 0–0.4 (raw data in the Supplemental Material [23]). To remove the Pr contribution, we employed a direct subtraction method [33,34] using the susceptibility of  $\text{Pr}^{3+}$  proposed by Tsubouchi *et al.* [35]:  $\chi^{\text{Pr}^{3+}}(T) = 1.6/(T + 54)$  emu/mol. Figure 9(a) displays the resulting curves reflecting the cobalt susceptibility  $\chi^{\text{Co}}$  for selected values of  $x$ . The  $T_{\text{SST}}$  and  $T_C$  temperatures were derived from a rise in  $\chi^{\text{Co}}(T)$  and a negative maximum in  $d\chi^{\text{Co}}/dT$  as  $T$  is increased, respectively (see details in the Supplemental Material [23]). The  $x$  dependencies of these characteristic temperatures are reported in the phase diagram of Fig. 9(c). These lines are well consistent with those previously reported by El-Khatib *et al.* [36], except that we did not find evidence of a SRO line  $\sim 250$  K (see the Supplemental Material [23]).

## IV. DISCUSSION

### A. Phase diagram

Apart from the SRO lines, the most salient features of the phase diagram of Fig. 6 are (i) existence of a  $y_{\text{crit}}$  separating two regimes, dominated either by FM or VSST; (ii) below  $y_{\text{crit}}$ , the  $T_C$  decreases as  $y$  increases; (iii) above  $y_{\text{crit}}$ , the  $T^*$  increases as  $y$  increases. These features are in line with previous results of the literature on VSST. In  $(\text{Pr}_{1-y}\text{Sm}_y)_{0.7}\text{Ca}_3\text{CoO}_3$ ,

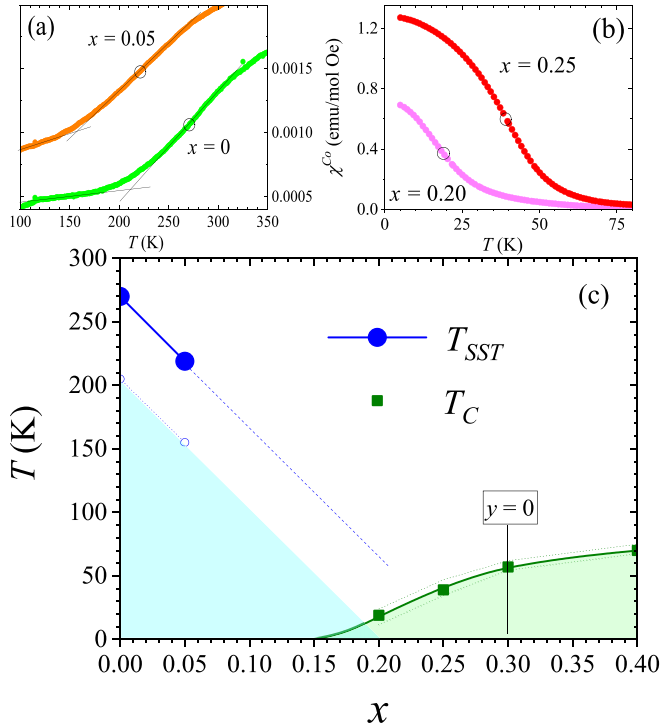


FIG. 9. Magnetic investigation of the  $\text{Pr}_{1-x}\text{Ca}_x\text{CoO}_3$  series. (a) and (b) Susceptibility curves recorded in 0.1 T for selected  $x$  values. The contribution from the  $\text{Pr}^{3+}$  ions has been removed to isolate the Co response (see text). Panel (a) refers to the low- $x$  range, in which the rise in  $\chi^{\text{Co}}(T)$  is associated with the spin-state transition (SST) of  $\text{Co}^{3+}$  from low spin (LS) to high spin (HS). The characteristic  $T_{\text{SST}}$  is associated with the midpoint of the transition (circles), while the beginning of the SST is derived from the crossing point between two linear extrapolations of  $\chi^{\text{Co}}(T)$ . Robust signature of these features is no longer discernable for  $x > 0.05$ . Panel (b) corresponds to the high- $x$  regime where a clear ferromagnetic (FM) response takes place. The  $T_C$  is derived from the point of maximum slope in  $\chi^{\text{Co}}(T)$  (circles). Panel (c) displays these temperatures as a function of  $x$ , which represents the fraction of tetravalent cobalt. Also shown are the beginning of the SST (open circles) and maxima in  $\partial^2(\chi^{\text{Co}})/\partial T^2$  on the FM side (dotted green lines) which reflect the width of the Curie transition. The blue dashed line is an extrapolation of the  $T_{\text{SST}}(y)$  line, aimed to materialize the interplay with the FM regime.

Fujita *et al.* [8] showed that the SST (the valence character of the transition being unknown at that time) takes place at a temperature that increases as  $y$  is increased from  $y \sim 0.2$  to 0.8; the lower boundary was ill defined, but there was no SST for  $y = 0.1$ . Soon after, Wang *et al.* [37] explored the same system with increased resolution in  $y$ , and they found a FM/SST boundary at  $y_{\text{crit}} \sim 0.175$ . Investigation of the closely related  $(\text{Pr}_{1-y}\text{Eu}_y)_{0.7}\text{Ca}_3\text{CoO}_3$  showed the same qualitative behavior, with  $y_{\text{crit}} \sim 0.19$  [11]. The most studied system in VSST literature is  $(\text{Pr}_{1-y}\text{Y}_y)_{0.7}\text{Ca}_3\text{CoO}_3$ , owing to the fact that  $\text{Y}^{3+}$  is nonmagnetic, which facilitates the analysis [10,14,27,30,32,38–40]. However, the size difference with  $\text{Pr}^{3+}$  is quite strong [41], which makes it difficult to follow the emergence of the VSST. In this system, Hejtmanek *et al.* [6] found that the lowest  $y$  value of their series ( $y = 0.0625$ ) is

enough to switch the system into the VSST regime. In a later study [30], it was shown that  $y_{\text{crit}}$  is still lower, i.e.,  $< 0.05$ . In practice, no compound characteristic of the FM regime was reported in  $(\text{Pr}_{1-y}\text{Y}_y)_{0.7}\text{Ca}_3\text{CoO}_3$  for  $y \neq 0$ . In this paper on the  $(\text{Pr}_{1-y}\text{Sm}_y)_{0.7}\text{Ca}_3\text{CoO}_3$  system, we have the advantage of a quite complete phase diagram, encompassing the FM and VSST regimes and allowing a fine inspection of the crossover between them.

### 1. Crossover FM/V SST: $y_{\text{crit}}$

Phelan *et al.* [30] emphasized that the emergence of a  $\text{Pr}^{4+}$  fraction in VSST compounds can shift the  $\text{Co}^{4+}/\text{Co}^{3+}$  ratio below the threshold for FM. To investigate this issue in detail, let us consider the phase diagram established for  $\text{Pr}_{1-x}\text{Ca}_x\text{CoO}_3$  [Fig. 9(c)] and the  $\text{Pr}^{4+}$  ( $y$ ) plot of Fig. 8. The  $\text{Pr}^{4+}$  content exhibits a jump around  $y_{\text{crit}} = 0.18$ . The low  $y$  side of this jump corresponds to  $y = 0.175$  (with an average Pr valence of 3.06), a composition for which the main transition is a  $T_C$  (see Fig. 6). It corresponds to an amount of  $\text{Pr}^{4+}$  per formula unit—noted  $[\text{Pr}^{4+}]$ —given by  $0.06 \times 0.7 \times (1 - 0.175) = 0.035$ , and thus an amount of  $\text{Co}^{4+}$  per formula unit equal to  $(0.3 - 0.035) = 0.265$ . In Fig. 9, one can see that, for such a doping level (keeping in mind that  $x$  corresponds to the ratio  $\text{Co}^{4+}/\text{Co}$ ), the FM regime is clearly dominant, with  $T_C > T_{\text{SST}}$  (if any). In Fig. 8, the high- $y$  side of the jump in  $\text{Pr}^{4+}$  ( $y$ ) corresponds to  $y = 0.20$  (Pr valence 3.15), for which the main transition has now turned into a VSST (see Fig. 6). This  $y$  value corresponds to  $[\text{Pr}^{4+}] = 0.084$  and thus  $[\text{Co}^{4+}] = 0.216$ . It turns out that this latter value lies in a range of doping where one can speculate that the hierarchy between FM and VSST has been reversed, i.e.,  $T_{\text{SST}} > T_C$  [Fig 9(c)]. In the end, it thus appears that the jump in  $\text{Pr}^{4+}$  ( $y$ ) is remarkably consistent with the phase diagram of  $(\text{Pr}_{1-y}\text{Sm}_y)_{0.7}\text{Ca}_3\text{CoO}_3$  when considering the influence of the doping level ( $\text{Co}^{4+}/\text{Co}$ ) on the hierarchy between SST and FM ordering.

### 2. $T_C$ vs $y$

First, one must address the FM nature in the low  $y$  range. This issue is still intensively debated in the prototypical case of  $y = 0$ . It was claimed that  $\text{Pr}_{0.7}\text{Ca}_{0.3}\text{CoO}_3$  is not a genuine FM [42] and that its magnetism is inhomogeneous [35]. Possibilities of a phase-separated (PS) state [42] or of a spin glass [43] were proposed, but the question has remained unsolved. More recently, experimental data reactivated the controversy, particularly spectra of small-angle neutron scattering [36] and the analysis of Schottky terms in heat capacity measurements [28]. The former was found to support a model of PS, whereas the latter led to a claim of homogeneous magnetism. Overall, our data rather lend support to a PS picture, one of the most significant arguments being the absence of a clear peak in  $C(T)$ , while there is a sharp rise in  $\chi(T)$  upon cooling. We consider this is not compatible with a bulk FM involving 100% of the volume. It remains that there is a very clear FM-like response and that the domains in which it develops can be quite large [30].

About the dependence  $T_C(y)$ , it is known that a decrease in  $\langle r_A \rangle$  reduces the Co-O-Co angle, which in turn opposes the setting of a FM state (via DE) [28,44,45]. This effect is present when increasing the content of  $\text{Sm}^{3+}$  that

has a smaller ionic radius than  $\text{Pr}^{3+}$ . As  $y$  is increased, it is thus expected to observe a decrease in the temperature of FM ordering, both for the  $T_C$  and  $T_{\text{SRO}}$  lines (which exhibit the same slope vs  $y$  in Fig. 6). To be more quantitative, let us consider the literature on cobaltates. Considering  $\text{RE}_{0.7}\text{AE}_{0.3}\text{CoO}_3$ , we collected data of  $T_C$  vs  $\langle r_A \rangle$  for various RE elements and alkaline-earth metals [28,46]. These data are found to obey a linear law within the relevant range of cationic radius:  $dT_C/d\langle r_A \rangle = 2734 \text{ K}/\text{\AA}$  (see the Supplemental Material [23]). In the  $(\text{Pr}_{1-y}\text{Sm}_y)_{0.7}\text{Ca}_3\text{CoO}_3$  series, the dependence of  $\langle r_A \rangle$  vs  $y$  is linear too:  $d\langle r_A \rangle/dy = 0.7[r_A(\text{Sm}^{3+}) - r_A(\text{Pr}^{3+})] = -0.0329 \text{ \AA}$ . Therefore, we anticipate a slope  $dT_C/dy = (dT_C/d\langle r_A \rangle)(d\langle r_A \rangle/dy) = -90 \text{ K}$ , which is plotted in Fig. 6. It turns out that the experimental  $dT_C/dy$  is in good agreement with this value. This supports the idea that the FM signatures in this system (including SRO) are related to the DE mechanism.

### 3. $T^*$ vs $y$

In the VSST regime above  $y_{\text{crit}}$ , one observes that  $T^*$  increases as a function of  $y$ . One expects the position of  $T^*$  to be linked to the gap of the SST ( $\text{Co}^{3+}$  LS toward  $\text{Co}^{3+}$  HS), which depends not only on the crystalline electric field (CEF) but also on the cobalt bandwidth ( $W$ ), as evidenced by the isotopic effect ( $^{16}\text{O}/^{18}\text{O}$ ) in  $y = 0.3$  [37]. It was suggested that one should consider as the SST gap the quantity  $\Delta_{\text{SST}} = (\Delta_{\text{CEF}} - \Delta_{\text{Hund}}) - (W/2)$ , where  $\Delta_{\text{Hund}}$  is the Hund coupling energy, while  $W$  is proportional to the Co-Co transfer energy, which itself varies as the angle Co-O-Co [47].

Increasing,  $y$  in  $(\text{Pr}_{1-y}\text{Sm}_y)_{0.7}\text{Ca}_3\text{CoO}_3$  induces a decrease in  $\langle r_A \rangle$ , which in turn decreases the distance Co-O and the angle Co-O-Co. As a consequence,  $\Delta_{\text{SST}}$  is expected to increase, owing to both a larger  $\Delta_{\text{CEF}}$  (via decreasing Co-O) and a smaller  $W$  (via decreasing Co-O-Co). This dual effect can explain the increase of  $T^*$  as  $y$  is increased. Quantitatively, it must be emphasized that the angle effect strongly dominates over the distance one [7,8]. One can also note that the impact of an increase in Co-O-Co on  $T_{\text{SST}}$  is not linear [48], which is in good accordance with the observed rounded shape of  $T^*(y)$  in Fig. 6.

### 4. CW regime at high temperature

Another aspect of the evolution of magnetism along the  $(\text{Pr}_{1-y}\text{Sm}_y)_{0.7}\text{Ca}_3\text{CoO}_3$  series is the decrease of susceptibility at high temperature as  $y$  increases (see inset of Fig. 2). To isolate the Co response, one must first remove the contributions from Pr and Sm. For the former, we used the susceptibility measured on  $\text{Pr}_{0.7}\text{Ca}_{0.3}\text{Ga}_{0.7}\text{Ti}_{0.3}\text{O}_3$  [representative of  $\chi(\text{Pr}^{3+})$  in conditions very close to ours) and, for the latter, the expression derived from  $\text{SmCoO}_3$  by Ivanova *et al.* [49] [ $\chi(\text{Sm}^{3+}) = (1.4 \times 10^{-3} + 0.0276/T) \text{ emu/mol}$ ]. Then one needs to consider the diamagnetic component  $\chi_{\text{dia}} = -0.63 \times 10^{-4} \text{ emu/mol}$  as well as a temperature-independent term, referred to as  $\chi_0$ . This  $\chi_0$  incorporates several contributions, among which the most important are Pauli and van Vleck terms [50,51]. To complement the magnetic data, XAS experiments were carried out to investigate the  $\text{Co}^{3+}$  spin state at room temperature [52]. It was found that the nature of the HS/LS mixture is only slightly affected by the  $y$  value

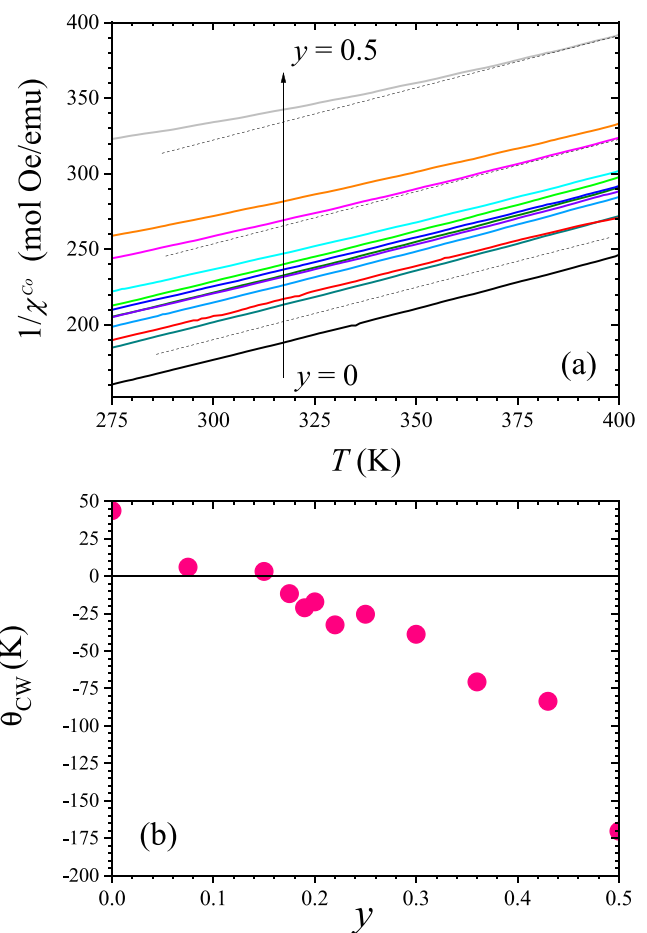


FIG. 10. Reciprocal Co susceptibility at high temperatures, for all the  $y$  values. The dashed lines have the slope derived from the curve of  $y = 0$ . (b) Curie-Weiss (CW) temperatures as a function of  $y$ , when using the  $\chi^{\text{Co}}$  susceptibility of (a) and assuming a  $\text{Co}^{3+}$  spin state independent of the Sm content at room temperature.

in this  $T$  range (see the Supplemental Material [23]). The fitting of the XAS spectra yields a percentage  $\text{Co}^{3+}\text{HS}/\text{Co}$  at room temperature of  $\sim 42$ ,  $37$ , and  $34\%$  for  $y = 0$ ,  $0.3$ , and  $0.36$ , respectively. To get  $\mu_{\text{eff}}$  consistent with these XAS results, we needed to set  $\chi_0 = 5 \times 10^{-4} \text{ emu/mol}$ , which lies within the range of expected values (see the Supplemental Material [23]). In the end, our estimate of the cobalt susceptibility  $\chi^{\text{Co}}$  at high temperature is obtained by calculating the following:

$$\chi^{\text{Co}}(y, T) = \chi(y, T) - 0.7(1-y)\chi(\text{Pr}^{3+}, T) - 0.7y\chi(\text{Sm}^{3+}, T) - \chi_{\text{dia}} - \chi_0. \quad (1)$$

The reciprocal susceptibility curves [Fig. 10(a)] show the persistence of an upward shift as  $y$  is increased, demonstrating that this feature is intrinsic to the Co response and does not only come from the difference in magnetism between  $\text{Pr}^{3+}$  and  $\text{Sm}^{3+}$ . On closer inspection, one also observes that the  $1/\chi^{\text{Co}}(T)$  curves tend to exhibit a concave upward shape for the highest  $y$  values. However, these curves correspond to the lowest  $\chi$  values, so they are expected to be the most affected by the experimental uncertainties; since the XAS experiments at room temperature have shown that the ratio  $\text{Co}^{3+}\text{HS}/\text{Co}$  is



weakly affected by  $y$ , we made a CW analysis of the curves in Fig. 10(a) by assuming the same slope for all of them (so just reducing the fitting range for highest  $y$  values). Figure 10(b) displays the  $\theta_{CW}$  derived in such a way, from the linear intercepts to the temperature axis. As  $y$  is increased, one observes a continuous decrease in  $\theta_{CW}$  with a striking change in sign from positive to negative.

Within the  $(\text{Pr}_{1-y}\text{Sm}_y)_{0.7}\text{Ca}_3\text{CoO}_3$  system, the magnetic interactions bring into play a competition between a DE mechanism involving  $\text{Co}^{4+}\text{LS}/\text{Co}^{3+}\text{HS}$ , and superexchange (SE) couplings dominated by the one associated with  $\text{Co}^{3+}\text{HS}/\text{Co}^{3+}\text{HS}$ . For a matter of the Co-O-Co angle, the FM DE mechanism is progressively weakened as  $y$  is increased, which thus enhances the signature of the SE interaction  $\text{Co}^{3+}\text{HS}/\text{Co}^{3+}\text{HS}$ , which is antiferromagnetic. This phenomenon can explain the observed crossover between positive and negative  $\theta_{CW}$  values as a function of  $y$ . We note that a similar behavior was previously reported in  $\text{La}_{1-x}\text{Ca}_x\text{CoO}_3$  [53]. Let us also add that the  $\theta_{CW}$  for the largest  $y = 0.5$  ( $-175$  K) becomes close to that of  $\text{LaCoO}_3$ , whose estimates span a range from  $-160$  to  $-250$  K [50,53–56]. This can be ascribed to the fact that DE is virtually quenched for such a large  $y = 0.5$ , while the SE  $\text{Co}^{3+}\text{HS}/\text{Co}^{3+}\text{HS}$  in our compounds corresponds to a ratio  $\text{Co}^{3+}\text{HS}/\text{Co} \sim 40\%$ , which is very similar to the situation in  $\text{LaCoO}_3$ .

### 5. Nature of the SRO features

In this paper, SRO features have been identified both in the FM and VSST regimes. Note that we prefer to keep the denomination SRO even though it was reported that some of the clusters can spread over rather large length scales, reaching several tens of angstroms [36]. The basic question to be addressed is the nature of these clusters and the associated FM.

To do so, let us consider the case of  $y = 0$  ( $\text{Pr}_{0.7}\text{Ca}_{0.3}\text{CoO}_3$ ). From XMCD of Co at 5 K (see the Supplemental Material [23]), we isolated the magnetic response of Co, which yields a  $\mu^{\text{Co}}(B)$  very well consistent with that derived when subtracting the Pr signal from a  $M(B)$  curve [27]. The shape at low  $B$  is the one displayed in Fig. 5(a); increasing the field  $>2$  T confirms the absence of saturation up to 9 T (XMCD) and even up to 14 T (magnetization). While the remanent magnetization of  $0.3 \mu_B$  per Co could well correspond to the response of  $\text{Co}^{4+}\text{LS}$  ( $S = \frac{1}{2}$ ) [27,28], the larger values of magnetization observed in high field are problematic. Basically, this is incompatible with a scheme where all the  $\text{Co}^{3+}$  are LS, so one has to consider that a fraction of them is in a higher spin state. About the alternative between intermediate or HS states for  $\text{Co}^{3+}$ , our previous studies lead us to favor the second possibility, with a mixture LS/HS [15,18]. Following similar reasoning, Knížek *et al.* [27] suggested the existence of a small fraction of  $\text{Co}^{3+}\text{HS}$  related to oxygen defects. Considering that  $\text{Pr}_{0.7}\text{Ca}_{0.3}\text{CoO}_3$  is on the borderline of a SST (LS/HS), such a small fraction of  $\text{Co}^{3+}\text{HS}$  at  $T \ll T_{\text{SST}}$  could also simply be regarded as a mark of the low- $T$  tail of the transition. The clusters would correspond to the zones around these  $\text{Co}^{3+}\text{HS}$ , into which the coexistence with  $\text{Co}^{4+}\text{LS}$  neighbors can trigger FM interaction via DE. Accordingly,

the SRO would mark the FM ordering of these clusters, leading to a PS state since these clusters are embedded into a non-FM matrix where the  $\text{Co}^{3+}$  are LS.

In  $\text{Pr}_{0.7}\text{Ca}_{0.3}\text{CoO}_3$ , the increase in susceptibility as  $T$  is decreased is very broad, indicating an inhomogeneous magnetic ordering of the clusters. The most likely reason is the statistical variety of local configurations involving  $(\text{Co}^{4+}\text{LS}/\text{Co}^{3+}\text{HS}/\text{Co}^{3+}\text{LS})$  which can induce a broad distribution of SRO temperatures. In such a vision, the temperature we referred to as the  $T_C$  should be regarded as the value of Curie temperature associated with the most probable local configuration of cobalt cations.

Turning back to the  $\mu^{\text{Co}}(B)$  curve at low  $T$ , we claim it can be described by the combination of two mechanisms: alignment of FM domains and polarization of the background. The former is associated with the clusters involving the couple  $(\text{Co}^{3+}\text{HS}/\text{Co}^{4+}\text{LS})$ , and it is responsible for the hard FM features, i.e., remanence and coercivity; the latter is associated with the surrounding matrix involving  $(\text{Co}^{3+}\text{LS}/\text{Co}^{4+}\text{LS})$ , and it is responsible for the smooth increase of magnetization as the field is increased. Using rough spin-only estimates of the magnetic moments for  $\text{Co}^{3+}\text{HS}$  ( $4 \mu_B$ ) and  $\text{Co}^{4+}\text{LS}$  ( $1 \mu_B$ ), the assumption of a fraction  $\text{Co}^{3+}\text{HS}/\text{Co}^{3+}$  equal to  $\sim 10\%$  would lead to a saturation magnetization of  $(0.7 \times 0.1 \times 4) + (0.3 \times 1) = 0.58 \mu_B$ , compatible with XMCD and magnetization data.

The above description of FM clusters is also relevant to the VSST side of the phase diagram, both for  $T_{\text{SRO}}$  and  $T_C$ -like lines. For each of them, one observes that their portions on the two sides of  $y_{\text{crit}}$  are located in the continuation of one another, but there is a downward shift when entering the VSST regime. This originates from the fact that the VSST induces a decrease in the doping level ( $\text{Co}^{4+}/\text{Co}$ ), which yields in turn a decrease in the temperature of FM ordering [see Fig. 9(c)].

The MR can be useful to shed light on the nature of SRO [30]. Let us focus here on the ground state that was investigated by MR measurements at 5 K. On the VSST side (large  $y$  values), the large negative MR is consistent with what is expected in PS systems involving metallic FM clusters. Quantitatively, one can even note that  $-15\%$  in 9 T for  $y = 0.43$  is close to what is observed in  $(\text{Pr}_{0.9}\text{Y}_{0.1})_{0.7}\text{Ca}_{0.3}\text{CoO}_3$  for similar values of  $T^*$  [30]. Supporting the similarity with Ref. [30], we also observed hysteresis in the  $\text{MR}(B)$  curves ( $\sim \pm 0.2$  T around zero field), which is consistent with a vision of intercluster negative MR. In contrast, the MR in the FM regime (being both lower in absolute value and positive) is much more puzzling.

Positive MR is quite rare in transition metal oxides. In a study on  $\text{La}_{1-x}\text{Ca}_x\text{CoO}_3$  for  $x \sim 0.25$ , similar results were reported, but no clear conclusion could be reached about the origin of this positive MR [57]. Various possible origins for such positive MR at low  $T$  in oxides are reviewed in Ref. [57], but none of them can be unambiguously applied to our data. Moreover, in the present case of  $(\text{Pr}_{1-y}\text{Sm}_y)_{0.7}\text{Ca}_3\text{CoO}_3$  compounds, Fig. 5(b) shows a change in the curvature of  $\text{MR}(B)$  as the field is increased, pointing to a competition between (at least) two mechanisms of opposite signs [58]. One can be reasonably confident about the nature of only one of them, i.e., the negative MR present in the VSST samples (large

$y$  values) which can likely be ascribed to a mechanism of tunneling between FM clusters within a non-FM matrix. As for the positive MR, we suggest it might result from the very peculiar type of PS in low  $y$  compositions, where the density (and maybe also the size) of FM clusters is much higher than for high  $y$ .

### B. Structural origin of the Pr mixed valence

A central issue for the understanding of the VSST is the origin of the stabilization of a  $\text{Pr}^{4+}$  fraction at low  $T$ . First, it can be recalled that Pr is prone to exhibit mixed valence (3+/4+) including in oxides, e.g., in  $\text{Pr}_6\text{O}_{11}$ . If focusing attention to the case of a perovskite, the best-known example is that of  $\text{BaPrO}_3$ , where Pr sits on the B sites. Mixed valence was also found with Pr on the A sites, for instance, in  $\text{PrSc}_{1-x}\text{Mg}_x\text{O}_3$  [59] or even in  $\text{PrAlO}_3$ , depending on the annealing conditions [60]. What is striking in the  $(\text{Pr}_{1-y}\text{Sm}_y)_{0.7}\text{Ca}_3\text{CoO}_3$  series is that the mixed valence only takes place below a certain transition temperature. To the best of our knowledge, there is only one previous case of that type, occurring in the double perovskite  $\text{Ba}_2\text{PrRu}_{1-x}\text{Ir}_x\text{O}_6$  (for  $0.1 \leq x \leq 0.4$ ), where it is related to the interplay between  $\text{Ru}^{5+}$  and  $\text{Ir}^{4+}$  [61,62].

In  $(\text{Pr}_{1-y}\text{RE}_y)_{1-x}\text{Ca}_x\text{CoO}_3$ , Naito *et al.* [9] carried out a comprehensive study over broad ranges of  $x$ ,  $y$ , and various RE, to identify the structural parameters allowing us to observe VSST. It was concluded that it requires small enough  $r_A$  and some minimum degree of disorder in size, quantified by the atomic randomness  $\sigma^2 = \sum_i z_i r_i^2 - \langle r_A \rangle^2$ , where  $z_i$  and  $r_i$  are the concentration and ionic radius of each element in the A site, respectively [9]. Since VSST is intimately connected to the mixed valence of Pr, these criteria might be regarded as those necessary to induce a fraction of  $\text{Pr}^{4+}$  at low  $T$ . Note, however, that this approach could not account for the VSST in the archetypical compound  $\text{Pr}_{0.5}\text{Ca}_{0.5}\text{CoO}_3$  for which  $\sigma^2$  is very small.

The latest studies on cobaltates have suggested that the underlying parameter controlling the appearance of  $\text{Pr}^{4+}$  is rather the bond angle Co-O-Co. The apparent link between the VSST and the couple  $(r_A, \sigma^2)$  can be ascribed to the fact that Pr/RE substitution is in practice the easiest way to reduce this angle. It was also shown that the distortion of the  $\text{CoO}_6$  octahedra plays a role in itself, in such a way that an average value of Co-O-Co is only relevant in first approximation [63]. Comparing the structural parameters of  $\text{Pr}_{0.5}\text{Ca}_{0.5}\text{CoO}_3$  (VSST),  $\text{Pr}_{0.55}\text{Ca}_{0.45}\text{CoO}_3$  (no VSST), and  $\text{Pr}_{0.50}\text{Y}_{0.05}\text{Ca}_{0.45}\text{CoO}_3$  (VSST), García-Muñoz *et al.* [3] claimed a leading role of the apical tilting of the  $\text{CoO}_6$  octahedra, suggesting that the corresponding  $\theta_1$  angle should be  $< \sim 158^\circ$  to allow the stabilization of a  $\text{Pr}^{4+}$  fraction at low  $T$ . Later, it was confirmed that such a critical angle can be consistent with the appearance of VSST for  $x > 0.45$  within the fully oxygenated  $\text{Pr}_{1-x}\text{Ca}_x\text{CoO}_3$  series [44]. In this paper on  $(\text{Pr}_{1-y}\text{Sm}_y)_{0.7}\text{Ca}_{0.3}\text{CoO}_3$ , however, Fig. 1(b) shows that the  $\theta_1$  corresponding to  $y_{\text{crit}} \sim 0.18$  is noticeably lower, i.e.  $\sim 157.2^\circ$ . At this stage, it is difficult to know whether this discrepancy is just a matter of experimental uncertainties, or if it rather indicates that the complexity of the charge transfer in these cobaltates cannot be reduced to a single angle, inde-

pendently of other important parameters such as the doping level.

### C. Chemical composition and VSST

Experimentally, the VSST has been observed only in perovskites of formula  $\text{ACoO}_3$ , with Pr and Ca on the A sites. We have seen that the basic ingredients to get a VSST are the existence—at low  $T$ —of RE in a mixed valence and of  $\text{Co}^{3+}$  in the LS state. Strikingly, it turns out that this RE can only be Pr in practice [13,64]; none of the other RE susceptible to exhibit a mixed valence (e.g., Tb) can in itself trigger the VSST [12]; it is probably a matter of hybridization with the O  $2p$  orbitals and respective positioning of the RE and Co bands [13]. On the basis of electronic-structure calculations, Knížek *et al.* [13] evidenced the existence of a broad Pr  $4f^2$  band located just below the Fermi level of  $\text{Pr}_{0.5}\text{Ca}_{0.5}\text{CoO}_3$ ; replacing Pr by its closest neighbor Nd makes this feature disappear.

Therefore, the set of conditions to get VSST can be rewritten as (i) presence of Pr at the A sites, (ii) mixed valence  $\text{Co}^{3+}/\text{Co}^{4+}$  to accommodate the change in Pr valence, and (iii) average A site radius below a limit value to get Co-O-Co small enough to stabilize at low  $T$  the  $\text{Co}^{3+}$  in LS state and a fraction of  $\text{Pr}^{4+}$ . In practice (ii) requires the incorporation of a divalent alkaline-earth metal, and (iii) requires that it is  $\text{Ca}^{2+}$  since obeying this size condition is impossible with other usual divalent cations, like  $\text{Sr}^{2+}$  or  $\text{Ba}^{2+}$ . Finally, the combination of these various requirements to get VSST shows it is natural that this peculiar transition was observed only in  $(\text{Pr,Ca})\text{CoO}_3$  perovskites.

## V. CONCLUSIONS

Investigation of several physical properties led us to build a phase diagram of the system  $(\text{Pr}_{1-y}\text{Sm}_y)_{0.7}\text{Ca}_{0.3}\text{CoO}_3$  ( $0 < y < 0.5$ ), tracking the variations of the VSST temperature  $T^*$ , the Curie temperature  $T_C$ , and the FM SRO ( $T_{\text{SRO}}$ ). This diagram exhibits a competition between a FM regime (low  $y$ ) and a VSST regime (high  $y$ ), with a crossover between them taking place around  $y_{\text{crit}} \sim 0.18$ .

The first basic question is the origin of  $y_{\text{crit}}$ , an issue for which XAS quantifying the variation of  $\text{Pr}^{4+}$  vs  $y$  was decisive. The ratio  $\text{Pr}^{4+}/\text{Pr}$  is shown to increase from 0 ( $y = 0$ ) to  $\sim 0.3$  ( $y = 0.5$ ), with an acceleration around  $y_{\text{crit}}$ . It is along this jump that the  $\text{Pr}^{4+}/\text{Pr}^{3+}$  ratio reaches a value large enough to shift the  $\text{Co}^{4+}/\text{Co}^{3+}$  below the threshold for which  $T_C < T^*$ .

The second basic question is the underlying cause of such a stabilization of  $\text{Pr}^{4+}$ . We found that this phenomenon in  $(\text{Pr}_{1-y}\text{Sm}_y)_{0.7}\text{Ca}_{0.3}\text{CoO}_3$  corresponds to an apical Co-O-Co  $< \sim 157.2^\circ$ , i.e., a value significantly smaller than the one reported in compounds closer to half-doping [3]. Despite this discrepancy that remains to be investigated, there is no doubt that the Co-O-Co angles play a very central role in the VSST systems since they also control the variations of  $T_C(y)$  and  $T^*(y)$ .

In addition to the competition between FM and VSST transitions, we observed FM SRO over the whole  $y$  range, indicating the presence of diluted FM clusters. Their amount remains small, even in the FM-like regime, and it becomes

very tiny above  $y_{\text{crit}}$ . Both the  $T_C(y)$  and  $T_{\text{SRO}}(y)$  lines were found to be consistent with a standard DE mechanism. Our analysis led us to suggest that these FM signatures are associated with clusters involving  $\text{Co}^{4+}$  LS/ $\text{Co}^{3+}$  HS embedded in a background involving  $\text{Co}^{4+}$  LS/ $\text{Co}^{3+}$  LS.

Finally, it must be stressed that several features of the VSST remain puzzling. For instance, our data confirmed previous studies on the point that there is a  $y$  value for which the first-order character of the VSST seems to be enhanced [65]. The cause of such an optimum [ $y \sim 0.3$  for  $(\text{Pr}_{1-y}\text{Sm}_y)_{0.7}\text{Ca}_{0.3}\text{CoO}_3$ ] is not obvious. Is the  $\text{Pr}^{4+}$  fraction too small for smaller  $y$ ? Is the cooperativity between the Pr

and Co sublattices decreased for too large  $y$ ? These questions illustrate the fact that there is still much work to do before fully understanding the VSST in cobaltates.

#### ACKNOWLEDGMENTS

The authors acknowledge the ESRF for provision of synchrotron radiation facilities. Experiments at the ISIS Neutron and Muon Source were supported by the beamtime allocations XB2090092, XB2090093, XB2090094, XB2090095, and XB2090096 from the Science and Technology Facilities Council.

- 
- [1] S. Tsubouchi, T. Kyomen, M. Itoh, P. Ganguly, M. Oguni, Y. Shimojo, Y. Morii, and Y. Ishii, *Phys. Rev. B* **66**, 052418 (2002).
- [2] A. J. Barón-González, C. Frontera, J. L. García-Muñoz, J. Blasco, and C. Ritter, *Phys. Rev. B* **81**, 054427 (2010).
- [3] J. L. García-Muñoz, C. Frontera, A. J. Barón-González, S. Valencia, J. Blasco, R. Feyerherm, E. Dudzik, R. Abrudan, and F. Radu, *Phys. Rev. B* **84**, 045104 (2011).
- [4] J. Herrero-Martín, J. L. García-Muñoz, S. Valencia, C. Frontera, J. Blasco, A. J. Barón-González, G. Subías, R. Abrudan, F. Radu, E. Dudzik, and R. Feyerherm, *Phys. Rev. B* **84**, 115131 (2011).
- [5] J. Herrero-Martín, J. L. García-Muñoz, K. Kvashnina, E. Gallo, G. Subías, J. A. Alonso, and A. J. Barón-González, *Phys. Rev. B* **86**, 125106 (2012).
- [6] J. Hejtmánek, Z. Jiráček, O. Kaman, K. Knížek, E. Šantavá, K. Nitta, T. Naito, and H. Fujishiro, *Eur. Phys. J. B* **86**, 305 (2013).
- [7] T. Fujita, T. Miyashita, Y. Yasui, Y. Kobayashi, M. Sato, E. Nishibori, M. Sakata, Y. Shimojo, N. Igawa, Y. Ishii, K. Kakurai, T. Adachi, Y. Ohishi, and M. Takata, *J. Phys. Soc. Jpn* **73**, 1987 (2004).
- [8] T. Fujita, S. Kawabata, M. Sato, N. Kurita, M. Hedo, and Y. Uwatoko, *J. Phys. Soc. Jpn* **74**, 2294 (2005).
- [9] T. Naito, H. Sasaki, and H. Fujishiro, *J. Phys. Soc. Jpn* **79**, 034710 (2010).
- [10] J. Hejtmánek, E. Šantavá, K. Knížek, M. Maryško, Z. Jiráček, T. Naito, H. Sasaki, and H. Fujishiro, *Phys. Rev. B* **82**, 165107 (2010).
- [11] A. V. Kalinov, O. Yu. Gorbenko, A. N. Taldenkov, J. Rohrkamp, O. Heyer, S. Jodlauk, N. A. Babushkina, L. M. Fisher, A. R. Kaul, A. A. Kamenev, T. G. Kuzmova, D. I. Khomskii, K. I. Kugel, and T. Lorenz, *Phys. Rev. B* **81**, 134427 (2010).
- [12] H. Fujishiro, T. Naito, D. Takeda, N. Yoshida, T. Watanabe, K. Nitta, J. Hejtmánek, K. Knížek, and Z. Jiráček, *Phys. Rev. B* **87**, 155153 (2013).
- [13] K. Knížek, J. Hejtmánek, P. Novák, and Z. Jiráček, *Phys. Rev. B* **81**, 155113 (2010).
- [14] H. Fujishiro, T. Naito, S. Ogawa, N. Yoshida, K. Nitta, J. Hejtmánek, K. Knížek, and Z. Jiráček, *J. Phys. Soc. Jpn* **81**, 064709 (2012).
- [15] F. Guillou, Q. Zhang, Z. Hu, C. Y. Kuo, Y. Y. Chin, H. J. Lin, C. T. Chen, A. Tanaka, L. H. Tjeng, and V. Hardy, *Phys. Rev. B* **87**, 115114 (2013).
- [16] V. Hardy, F. Guillou, and Y. Bréard, *J. Phys.: Condens. Matter* **25**, 246003 (2013).
- [17] J. M. Chen, J. M. Lee, S. C. Haw, S. A. Chen, V. Hardy, F. Guillou, S. W. Chen, C. Y. Kuo, C. W. Pao, J. F. Lee, N. Hiraoka, H. Ishii, K. D. Tsuei, and Z. Hu, *Phys. Rev. B* **90**, 035107 (2014).
- [18] F. Guillou, K. Kummer, Y. Bréard, L. Hervé, and V. Hardy, *Phys. Rev. B* **95**, 174445 (2017).
- [19] R. I. Smith, S. Hull, M. G. Tucker, H. Y. Playford, D. J. McPhail, S. P. Waller, and S. T. Norberg, *Rev. Sci. Instrum.* **90**, 115101 (2019).
- [20] O. Arnold, J. C. Bilheux, J. M. Borreguero, A. Buts, S. I. Campbell, L. Chapon, M. Doucet, N. Draper, R. Ferraz Leal, M. A. Gigg, V. E. Lynch, A. Markvardsen, D. J. Mikkelsen, R. L. Mikkelsen, R. Miller, K. Palmen, P. Parker, G. Passos, T. G. Perring, P. F. Peterson *et al.*, *Nucl. Instrum. Methods Phys. Res. A* **764**, 156 (2014).
- [21] J. Rodriguez-Carvajal, *Physica B* **192**, 55 (1993).
- [22] A. Rogalev and F. Wilhelm, *Phys. Met. Metall.* **116**, 1285 (2015).
- [23] See Supplemental Material at <http://link.aps.org/supplemental/10.1103/PhysRevMaterials.6.014401> for details about the signature of  $T_C$  on the  $C(T)$  curves; the shape of the  $M(B)$  curves at low  $T$ ; the temperature dependence of the MR; the training and hysteretical effects at the VSST; the resistivity in the phase diagram, the criteria used to derive  $T_C$ ,  $T^*$ , and  $T_{\text{SRO}}$ ; the Co spin state at room temperature from XAS; the magnetic investigation of the system  $\text{Pr}_{1-x}\text{Ca}_x\text{CoO}_3$ ; the absence of signature of SRO around room temperature in  $\text{Pr}_{0.7}\text{Ca}_{0.3}\text{CoO}_3$ ;  $T_C$  vs  $\langle r_A \rangle$  in  $\text{RE}_{0.7}\text{AE}_{0.3}\text{CoO}_3$  perovskites; the CW response of Co in  $\text{Pr}_{0.7}\text{Ca}_{0.3}\text{CoO}_3$ ; the Co magnetism from XMCD; the MR in  $\text{Pr}_{0.7}\text{Ca}_{0.3}\text{CoO}_3$ ; and the structural parameters of  $(\text{Pr}_{1-y}\text{Sm}_y)_{0.7}\text{Ca}_{0.3}\text{CoO}_3$  derived from tofPND.
- [24] K. Kummer, A. Fondacaro, E. Jimenez, E. Velez-Fort, A. Amorese, M. Aspbury, F. Yakhou-Harris, P. van der Linden, and N. B. Brookes, *J. Synchrotron Radiat.* **23**, 464 (2016).
- [25] G. Y. Wang, X. H. Chen, T. Wu, G. Wu, X. G. Luo, and C. H. Wang, *Phys. Rev. B* **74**, 165113 (2006).
- [26] We present here the data for our highest field of 5 T to enhance the signal-to-noise ratio in the low susceptibility regime when approaching 400 K.
- [27] K. Knížek, J. Hejtmánek, M. Maryško, P. Novák, E. Šantavá, Z. Jiráček, T. Naito, H. Fujishiro, and C. de la Cruz, *Phys. Rev. B* **88**, 224412 (2013).
- [28] Z. Jiráček, J. Hejtmánek, K. Knížek, M. Maryško, P. Novák, E. Šantavá, T. Naito, and H. Fujishiro, *J. Phys.: Condens. Matter* **25**, 216006 (2013).

- [29] J. B. Goodenough, *J. Phys. Chem. Solids* **6**, 287 (1958).
- [30] D. Phelan, K. P. Bhatti, M. Taylor, S. Wang, and C. Leighton, *Phys. Rev. B* **89**, 184427 (2014).
- [31] M. Maryško, Z. Jiráček, K. Knížek, P. Novák, J. Hejtmánek, T. Naito, H. Sasaki, and H. Fujishiro, *J. Appl. Phys.* **109**, 07E127 (2011).
- [32] T. Naito, H. Fujishiro, T. Nishizaki, N. Kobayashi, J. Hejtmánek, K. Knížek, and Z. Jiráček, *J. Appl. Phys.* **115**, 233914 (2014).
- [33] J.-Q. Yan, J.-S. Zhou, and J. B. Goodenough, *Phys. Rev. B* **69**, 134409 (2004).
- [34] Y. Kobayashi, T. Mogi, and K. Asai, *J. Phys. Soc. Jpn* **75**, 104703 (2006).
- [35] S. Tsubouchi, T. Kyomen, M. Itoh, and M. Oguni, *Phys. Rev. B* **69**, 144406 (2004).
- [36] S. El-Khatib, S. Bose, C. He, J. Kuplic, M. Laver, J. A. Borchers, Q. Huang, J. W. Lynn, J. F. Mitchell, and C. Leighton, *Phys. Rev. B* **82**, 100411(R) (2010).
- [37] G. Y. Wang, T. Wu, X. G. Luo, W. Wang, and X. H. Chen, *Phys. Rev. B* **73**, 052404 (2006).
- [38] A. Ikeda, S. Lee, T. T. Terashima, Y. H. Matsuda, M. Tokunaga, and T. Naito, *Phys. Rev. B* **94**, 115129 (2016).
- [39] T. Moyoshi, K. Kamazawa, M. Matsuda, and M. Sato, *Phys. Rev. B* **98**, 205105 (2018).
- [40] D. Phelan, M. J. Krogstad, N. J. Schreiber, R. Osborn, A. H. Said, H. Zheng, and S. Rosenkranz, *Phys. Rev. B* **100**, 054101 (2019).
- [41] In a ninefold coordination, the ionic radii of  $\text{Pr}^{3+}$  and of  $\text{Y}^{3+}$  are 1.179 and 1.075 Å, respectively (while that of  $\text{Sm}^{3+}$  is 1.132 Å).
- [42] A. K. Kundu, E. V. Sampathkumaran, K. V. Gopalakrishnan, and C. N. R. Rao, *J. Magn. Magn. Mater.* **281**, 261 (2004).
- [43] A. K. Kundu, P. Nordblad, and C. N. R. Rao, *J. Solid State Chem.* **179**, 923 (2006).
- [44] D. Phelan, Y. Suzuki, S. Wang, A. Huq, and C. Leighton, *Phys. Rev. B* **88**, 075119 (2013).
- [45] I. Fita, R. Szymczak, R. Puzniak, I. O. Troyanchuk, J. Fink-Finowicki, Ya. M. Mukovskii, V. N. Varyukhin, and H. Szymczak, *Phys. Rev. B* **71**, 214404 (2005).
- [46] C. Leighton, D. D. Stauffer, Q. Huang, Y. Ren, S. El-Khatib, M. A. Torija, J. Wu, J. W. Lynn, L. Wang, N. A. Frey, H. Srikanth, J. E. Davies, K. Liu, and J. F. Mitchell, *Phys. Rev. B* **79**, 214420 (2009).
- [47] J.-S. Zhou, J.-Q. Yan, and J. B. Goodenough, *Phys. Rev. B* **71**, 220103(R) (2005).
- [48] M. Tachibana, T. Yoshida, H. Kawaji, T. Atake, and E. Takayama-Muromachi, *Phys. Rev. B* **77**, 094402 (2008).
- [49] N. B. Ivanova, N. V. Kazak, C. R. Michel, A. D. Balaev, and S. G. Ovchinnikov, *Phys. Solid State* **49**, 2126 (2007).
- [50] Z. Jiráček, J. Hejtmánek, K. Knížek, and M. Veverka, *Phys. Rev. B* **78**, 014432 (2008).
- [51] K. Knížek, Z. Jiráček, J. Hejtmánek, M. Veverka, M. Maryško, G. Maris, and T. T. M. Palstra, *Eur. Phys. J. B.* **47**, 213 (2005).
- [52] M. Medarde, C. Dallera, M. Grioni, J. Voigt, A. Podlesnyak, E. Pomjakushina, K. Conder, Th. Neisius, O. Tjernberg, and S. N. Barilo, *Phys. Rev. B* **73**, 054424 (2006).
- [53] J. C. Burley, J. F. Mitchell, and S. Short, *Phys. Rev. B* **69**, 054401 (2004).
- [54] M. A. Señaris-Rodríguez and J. B. Goodenough, *J. Solid State Chem.* **116**, 224 (1995).
- [55] K. Knížek, Z. Jiráček, J. Hejtmánek, and P. Novák, *J. Phys.: Condens. Matter* **18**, 3285 (2006); K. Knížek, Z. Jiráček, J. Hejtmánek, P. Henry, and G. André, *J. Appl. Phys.* **103**, 07B703 (2008).
- [56] M. J. R. Hoch, S. Nellutla, J. van Tol, E. S. Choi, J. Lu, H. Zheng, and J. F. Mitchell, *Phys. Rev. B* **79**, 214421 (2009).
- [57] S. M. Zhou, Y. Li, Y. Q. Guo, J. Y. Zhao, and L. Shi, *Appl. Phys. Lett.* **105**, 232408 (2014).
- [58] This is further supported by the variation of  $MR(B)$  as a function of temperature (see the Supplemental Material [23]).
- [59] K. Sekizawa, M. Kitagawa, and Y. Takano, *J. Magn. Magn. Mater.* **177**, 541 (1998).
- [60] M. Wencka, S. Vrtnik, M. Jagodič, Z. Jagličič, S. Turczynski, D. A. Pawlak, and J. Dolinšek, *Phys. Rev. B* **80**, 224410 (2009).
- [61] M. Wakeshima, Y. Izumiyama, Y. Doi, and Y. Hinatsu, *Solid State Commun.* **120**, 273 (2001).
- [62] J. Sannigrahi, D. T. Adroja, C. Ritter, W. Kockelmann, A. D. Hillier, K. S. Knight, A. T. Boothroyd, M. Wakeshima, Y. Hinatsu, J. F. W. Mosselmans, and S. Ramos, *Phys. Rev. B* **99**, 184440 (2019).
- [63] P. Tong, Y. Wu, B. Kim, D. Kwon, J. M. S. Park, and B. G. Kim, *Phys. Soc. Jpn* **78**, 034702 (2009).
- [64] Y. Kobayashi, Y. Terakado, and K. Asai, and H. Yasuoka, *J. Phys. Soc. Jpn* **83**, 104704 (2014).
- [65] V. Hardy, Y. Bréard, and F. Guillou, *J. Phys.: Condens. Matter* **33**, 095801 (2021).